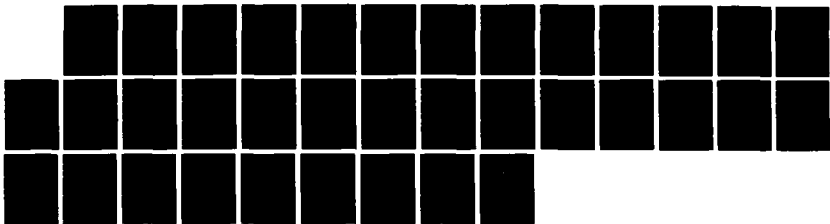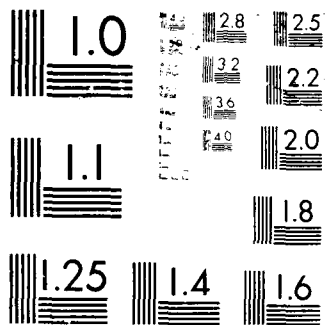AD-A193 026   THE PROPERTIES OF SOLAR CORONAL ACTIVE REGIONS DEDUCED   1/1
FROM X-RAY LINE SP..(U) AEROSPACE CORP EL SEGUNDO CA
SPACE SCIENCES LAB   D L MCKENZIE 05 FEB 88
UNCLASSIFIED   TR-0086A(2940-01)-1 SD-TR-88-04   F/G 3/2   NL
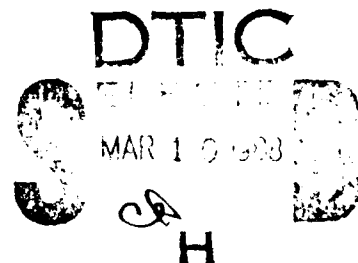
DTIC FILE COPY

AD-A193 026

The Properties of Solar Coronal Active Regions
Deduced from X-ray Line Spectra

D. L. McKENZIE
Space Sciences Laboratory
Laboratory Operations
The Aerospace Corporation
El Segundo, CA 90245

5 February 1988

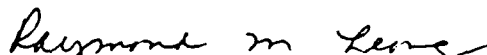DTIC

MAR 1 0 1988

H

88   3   5   084

This report was submitted by The Aerospace Corporation, El Segundo, CA 90245, under Contract No. F04701-85-C-0086 with the Space Division, P.O. Box 92960, Worldway Postal Center, Los Angeles, CA 90009. It was reviewed and approved for The Aerospace Corporation by H. R. Rugge, Director, Space Sciences Laboratory. Capt Kevin O'Brien, SD/CNS, was the project officer for the Mission-oriented Investigation and Experimentation (MOIE) Program.

This report has been reviewed by the Public Affairs Office (PAS) and is releasable to the National Technical Information Service (NTIS). At NTIS, it will be available to the general public, including foreign nationals.

This technical report has been reviewed and is approved for publication. Publication of this report does not constitute Air Force approval of the report's findings or conclusions. It is published only for the exchange and stimulation of ideas.

KEVIN O'BRIEN, Capt, USAF
MOIE Project Officer
SD/CNS

RAYMOND M. LEONG, Major, USAF
Deputy Director, AFSTC West Coast Office
AFSTC/WCO OL-AB

REPORT DOCUMENTATION PAGE

1a. REPORT SECURITY CLASSIFICATION	1b. RESTRICTIVE MARKINGS
Unclassified	

2a. SECURITY CLASSIFICATION AUTHORITY	3. DISTRIBUTION/AVAILABILITY OF REPORT
	Approved for public release;
2b. DECLASSIFICATION/DOWNGRADING SCHEDULE	distribution unlimited.

4. PERFORMING ORGANIZATION REPORT NUMBER(S)	5. MONITORING ORGANIZATION REPORT NUMBER(S)
TR-0086A(2940-01)-1	SD-TR-88-04

6a. NAME OF PERFORMING ORGANIZATION	6b. OFFICE SYMBOL (If applicable)	7a. NAME OF MONITORING ORGANIZATION
The Aerospace Corporation Laboratory Operations		Space Division

6c. ADDRESS (City, State, and ZIP Code)	7b. ADDRESS (City, State, and ZIP Code)
El Segundo, CA 90245	Los Angeles Air Force Base Los Angeles, CA 90009-2960

8a. NAME OF FUNDING/SPONSORING ORGANIZATION	8b. OFFICE SYMBOL (If applicable)	9. PROCUREMENT INSTRUMENT IDENTIFICATION NUMBER
		F04701-85-C-0086-P00016

8c. ADDRESS (City, State, and ZIP Code)	10 SOURCE OF FUNDING NUMBERS			
	PROGRAM ELEMENT NO.	PROJECT NO.	TASK NO.	WORK UNIT ACCESSION NO.

11 TITLE (Include Security Classification)

The Properties of Solar Coronal Active Regions Deduced from X-ray Line Spectra

12. PERSONAL AUTHOR(S)
McKenzie, D. L.

13a. TYPE OF REPORT	13b. TIME COVERED FROM _____ TO _____	14. DATE OF REPORT (Year, Month, Day) 1988, February 5	15. PAGE COUNT 30

16 SUPPLEMENTARY NOTATION

17 COSATI CODES			18 SUBJECT TERMS (Continue on reverse if necessary and identify by block number)
FIELD	GROUP	SUB-GROUP	Solar flares　　　　　　　Multigrid collimator
			SOLEX spectrometers　　　Nonflaring regions
			Crystal spectrometers

19 ABSTRACT (Continue on reverse if necessary and identify by block number)

Coronal active regions, the sites of energetic solar flares, have temperatures higher than 10^6 K and emit strongly in the X-ray region of the spectrum. In this report X-ray emission line-ratio diagnostics for electron density and temperature are applied to over 100 spectra of nonflaring active regions taken by the SOLEX B spectrometer aboard the U.S. Department of Defense Space Test Program's P78-1 Satellite from March to November 1979. The purpose is to draw general conclusions from analysis of the spectra of a large variety of regions.

The R ratio for O VII can be used to measure coronal electron densities when they exceed about 3×10^9 cm^{-3}. Only 8 of the 73 spectra for which the R ratio was measurable showed evidence of densities this high. For the remainder of the regions, the average R was 3.7, corresponding to a density of ~ 2×10^9 cm^{-3}. An independent density determination based on

20. DISTRIBUTION/AVAILABILITY OF ABSTRACT	21. ABSTRACT SECURITY CLASSIFICATION
☒ UNCLASSIFIED/UNLIMITED ☐ SAME AS RPT ☐ DTIC USERS	Unclassified

22a NAME OF RESPONSIBLE INDIVIDUAL	22b TELEPHONE (Include Area Code)	22c OFFICE SYMBOL

DD FORM 1473, 84 MAR　　83 APR edition may be used until exhausted
All other editions are obsolete

19. Abstract (Continued)

absolute line fluxes and the known area of the field of view yielded estimated lower-limit densities of $1.5-4.5 \times 10^9$ cm^{-3}. The agreement between these two independent density determinations gives confidence in current theoretical R-ratio calculations. Temperatures have been measured with the G ratios of O VII, Ne IX, and Mg XI and the ratio $R_1 = I(1s^2\ ^1S - 1s3p\ ^1P)/I(1s^2\ ^1S - 1s2p\ ^1P)$ for O VII and Ne IX. Use of ratios from these three species allows analysis of temperatures throughout the range to be found in nonflaring coronal active regions. The SOLEX data constrain the G-ratio range rather tightly; some of the existing calculations are not in acceptable agreement with observations. In addition to the solar G-ratio data, measured solar R_1 ratios and existing laboratory measurements have been used to resolve the inconsistencies in the theoretical calculations. The measured active-region temperatures are lower than the temperatures of most efficient production of the line emissions involved in the diagnostic ratios. This means that the emission-measure distribution is a decreasing function of temperature. In particular, the O VII temperatures are lower than 1.8×10^6 K, indicating that the emission-measure distribution function peaks at a temperature lower than this. This suggests that low-temperature ($< 2 \times 10^6$ K) loops are the predominant feature of nonflaring active regions.

CONTENTS

FIGURES

I. INTRODUCTION

This report contains the results of a study of the X-ray spectra of active regions in the solar corona. Coronal active regions, the sites of energetic solar flares, have plasma temperatures higher than 10^6 K and emit strongly in the X-ray region of the spectrum. X-ray emission-line-ratio diagnostics for electron density (Gabriel and Jordan 1969; McKenzie et al. 1980a) and temperature (Pradhan and Shull 1981; Keenan, Tayal, and Kingston 1984a,b,c; Keenan, Kingston, and McKenzie 1985,1986; Keenan et al. 1987) have been established in recent years. These diagnostics have been applied to over 100 spectra of nonflaring active regions taken by the SOLEX B Bragg crystal spectrometer aboard the U. S. Department of Defense Space Test Program P78-1 satellite. The purpose of the work is not to study some "average" active region, but to draw general conclusions from the analysis of the spectra of a large variety of regions.

The SOLEX B spectrometer has produced the first and only large set of active-region spectra. Prior to the launch of P78-1, active-region spectra were acquired during short rocket flights. Satellite-borne crystal spectrometers were uncollimated and concentrated on high-temperature flare emissions (Neupert et al. 1967; Doschek 1972) or observed only narrow regions of the spectrum (Siarkowski et al. 1982). Many of the early rocket investigations also used uncollimated spectrometers (Batstone et al. 1970) or concentrated on specific parts of the spectrum (Acton et al. 1972; Hutcheon, Pye, and Evans 1976a,b), but a few high-quality complete spectra were also obtained (Parkinson 1975). The SOLEX spectrometers were fitted with multigrid collimators specifically to allow observations of individual active regions or parts of them. The wavelength range of 7.7 to 23 Å allows the SOLEX B RAP (rubidium acid phthalate) spectrometer to measure emissions from plasmas at all temperatures above 1×10^6 K to be found in the solar corona. All of the data for this study were taken with the SOLEX B RAP spectrometer. The instrument is described by Landecker, McKenzie, and Rugge (1979) and McKenzie et al. (1980b).

The selection of data, both observational and theoretical, is of central importance to a study such as this. The observations selected for analysis must present a well-defined sample of nonflaring active regions. The selection of theoretical data is even more important. There exist a number of calculations of the diagnostic line ratios as a function of density and temperature. The calculations differ from one another enough that in many cases the interpretation of the data depends critically upon which theoretical data are deemed correct. One of the products of the study is a critical assessment, based on the solar data, of the accuracy of the various theoretical line-ratio calculations. The data selection for the study is discussed in Section II. The results of the study are presented in Section III, and Section IV interprets the results.

II. DATA SELECTION

A. OBSERVATIONAL DATA

The P78-1 satellite was launched in February 24, 1979 and the SOLEX spectrometers operated for approximately three years after that. However, a complete set of data tapes is available only for the period March-November 1979. All of the data for the study were acquired during this early period. A brief account of the data acquisition and selection is needed to describe the nature of the final data set.

The first step was taken during the P78-1 mission when it was decided where to point the spectrometers. The SOLEX B spectrometer was equipped with a one-arc-minute square (FWHM) multigrid collimator. Therefore, it was necessary to select, on a daily basis, what active region or part of an active region to observe; emissions from outside active regions were generally too weak to be detected. This choice was always driven by the aim of maximizing the probability of flare occurrence within the spectrometer's field of view, and was almost always made 12-36 hours in advance of the actual observations. As a result, the brightest and longest-lasting active regions tended to be selected for observation.

The aim of the final data selection was to obtain a wide sample of active-region spectra that were sufficiently intense that the data were usable. In addition, we were interested only in spectra from nonflaring regions. The absence of flaring in an active region under study was verified primarily by examining the data from the MONEX A low-energy monitor instrument, a full-disk-viewing x-ray proportional counter that was part of the P78-1 payload. When these data showed evidence of flaring, reference was made to Solar Geophysical Data to verify that any flare taking place was outside the spectrometer field of view.

What sort of data sample resulted from these selection procedures? To be sure, the procedures were biased toward selection of those active regions that were the brightest emitters of X rays. The data were also taken near the time

5

of solar maximum when one would expect x-ray emissions to be at their strong-
est. Nevertheless, there were significant periods in 1979 during which the
level of solar activity was low, and the data summary, in Table 1, shows that
a wide variety of regions was observed. A total of 111 spectra were selected
for analysis. Each spectrum was constructed by summing up to 13 consecutive
spectral scans over the wavelength range 7.7 to 23 Å. In the slow-scanning
mode that was used for most of the observations, a single scan took
169 seconds, so the data acquisition for a single spectrum took up to
2197 seconds.

B. THEORETICAL DATA

The primary aim of this work is to deduce the general properties of
coronal active regions by analyzing X-ray spectra. This is accomplished
through the use of three well-known diagnostic spectral-line ratios. Coronal
electron densities are determined from the ratio $R = f/i$ in O VII, where f
is the intensity of the forbidden $1s^2$ ^1S - $1s2s$ ^3S line and i is the
intensity of the intercombination $1s^2$ ^1S - $1s2p$ $^3P_{1,2}$ lines. The density
sensitivity of this ratio was first suggested by Gabriel and Jordan (1969); it
takes the form

$$n_e = n_c(R_0/R - 1) \tag{1}$$

where n_c and R_0 are theoretical parameters. Temperature diagnostics are
provided by the G ratio (Gabriel and Jordan 1969) and the R_1 ratio (Keenan,
Kingston, and McKenzie 1985,1986; Keenan et al. 1987). They are defined as
follows:

$$G = (f + i)/r \tag{2}$$

where r is the intensity of the $1s^2$ ^1S - $1s2p$ ^1P resonance line; and

$$R_1 = I(1s^2 \, ^1S - 1s3p \, ^1P)/r \tag{3}$$

where I stands for "intensity of." Use of these ratios for O VII, Ne IX, and
Mg XI allows us to analyze temperature distributions throughout the range that
characterizes nonflaring active regions.

Table 1. Summary of Active-Region Observations

Region	Start Date[a] 1979	End Date[a] 1979	Number of Spectra[a]	Comments
1638	Mar 23	Mar 25	3	M,X,2
1661	Mar 31	Apr 10	13	M,2
1689	Apr 20	Apr 23	3	M,2
1707	Apr 25	Apr 27	2	2
1705	Apr 28	Apr 28	1	M,X,2
1711	May 2	May 4	2	M
1724	May 9	May 10	2	
1734	May 10	May 12	2	
1761	May 25	May 25	1	
1776	Jun 1	Jun 1	1	
1781	Jun 6	Jun 13	10	M,X,2,3
1796	Jun 15	Jun 15	1	M,2
1819	Jun 25	Jun 25	1	
1840	Jun 29	Jul 12	8	
1849	Jul 13	Jul 13	1	2
1866	Jul 14	Jul 19	4	
1878	Jul 22	Jul 22	2	M
1880	Jul 23	Jul 25	2	M
1887	Jul 27	Jul 27	1	
1890	Jul 28	Aug 6	9	
1929	Aug 17	Aug 18	2	2
1943	Aug 19	Sep 2	9	M,X,2
1966	Sep 3	Sep 4	2	M
1994	Sep 19	Sep 28	8	M,X,2,3
2006/2021	Sep 29	Oct 4	5	
2032	Oct 5	Oct 16	8	2
2084	Nov 3	Nov 3	1	
2099	Nov 11	Nov 12	2	M,X,2
2106	Nov 16	Nov 18	4	M,2
2138	Nov 29	Nov 29	1	

[a]For observations reported in this report.

Comments--(M) Produced at least one class M X-ray burst. (X) Produced at least one class-X X-ray burst. (2) Produced at least one class-2 Hα flare. (3) Produced at least one class-3 Hα flare.

The active-region data presented here provide a means for assessing the accuracy of theoretical calculations of x-ray line strengths. Two of the ratios, R and G, have been calculated by a number of theoretical groups in recent years (Pradhan and Shull 1981; Pradhan 1982; Doyle, Tayal, and Kingston 1983; Wolfson et al. 1983; Keenan, Tayal, and Kingston 1984a,b,c), while R_1 has been calculated only by F. P. Keenan and his collaborators (Keenan, Kingston, and McKenzie 1985,1986; Keenan et al. 1987). The R-ratio calculations do not differ much from one another. All find $n_c \approx 3 \times 10^{10}$ cm^{-3} and $R_0 \approx 3.9$ at $T_m = 1.8 \times 10^6$ K, the temperature of most efficient O VII line emission. The data do provide a definitive test of the G-ratio calculations. The general conclusion, which will be developed in detail below, is that the latest and most sophisticated calculations are the most accurate. A number of the older theoretical predictions are found to be inconsistent with the data. Thus, the data provide a verification that real progress is being made in theoretical line-strength calculations.

III. RESULTS

A. ELECTRON DENSITY

The R ratio (equation 1) for O VII was used to determine the electron density. For each spectrum, line strengths in the wavelength range 21.35 - 22.29 Å were fitted with Voigt profiles (Finn and Mugglestone 1965) with a minimum χ^2 fitting criterion. A two-parameter fit to the "background" continuum was also made at the same time. Besides the three oxygen lines, the wavelength range is known to include the Ca XVI 2p $^2P_{1/2}$ - 3d $^2D_{3/2}$ line at 21.444 Å (McKenzie and Landecker 1982a). This line and three other possible lines at 21.94, 21.97, and 22.03 Å were initially included in the fits. The three unidentified lines were included because some evidence for their existence was found in early SOLEX flare spectra. Only the one at 22.03 Å has been detected with confidence in the SOLEX spectra (McKenzie and Landecker 1982a). The three lines are always weak in active-region spectra, and their existence or nonexistence does not significantly affect the measured R values. In the fitting procedure, the line strengths and background levels giving the minimum value of χ^2 were found by solving several simultaneous linear equations by a matrix-inversion technique. The number of degrees of freedom in the fits was 441-444, and the criterion for acceptability was $\chi^2 < 500$. This somewhat arbitrary criterion corresponds to a χ^2 probability of 97%.

By the above criterion, the oxygen line strengths were measurable for 73 of the spectra in the total data set of 111. For these spectra, the R values were determined from the count-rate ratios corrected for instrumental sensitivity. The fitting procedure gave the line strength and an error estimate for each line; therefore, it was possible to assign an uncertainty to each individual R determination. The histogram in Figure 1 summarizes the results. For the total data set, the mean value of R was 3.61. However, the data are not consistent with the conclusion that the R values are normally distributed about a mean of 3.61; the distribution is too broad. Since the R ratio is density sensitive, the lowest values may indeed arise from plasmas that have densities that are a significant fraction of n_c ($\sim 3 \times 10^{10}$ cm^{-3}).
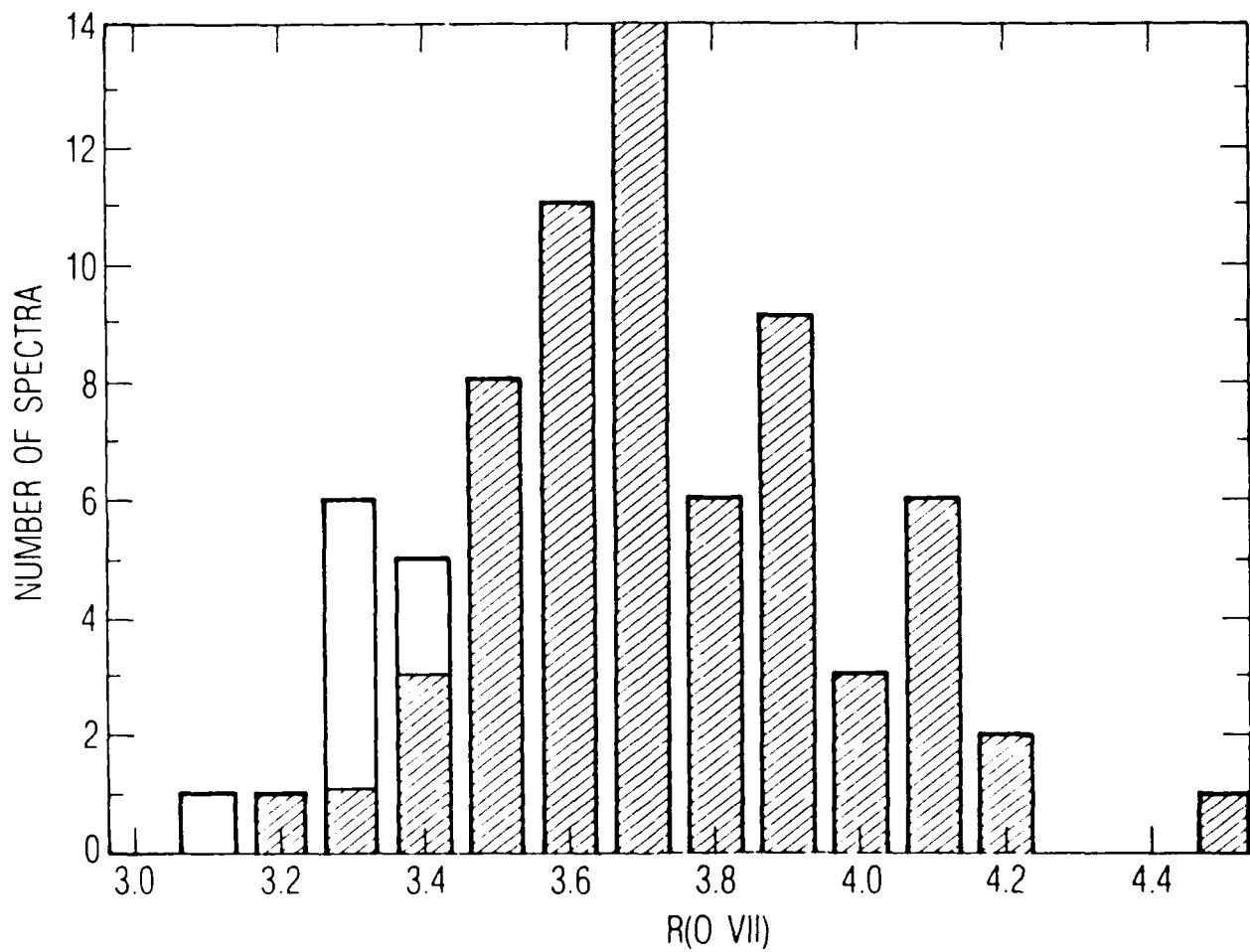
Figure 1. Frequency of Occurrence of R Ratios Plotted as a Function of R. Those that are cross-hatched had R + 2σ > 3.70 and are therefore in the low-density limit for R.

When all of the spectra for which $r + 2\sigma < 3.7$ are eliminated, the remaining R values are consistent with the assumption that R is normally distributed about a mean of 3.69. The resulting distribution is shown in Figure 1. The mean value of 3.69 is considerably smaller than the theoretical value of ~ 3.9 for the low-density limit at temperature T_m (Pradhan and Shull 1981; Pradhan 1982; Doyle, Tayal, and Kingston 1983; Keenan, Tayal, and Kingston 1984b). This is because the density is not zero but a small fraction of n_c, and so, by equation (1), $R < R_0$. For example, if R_0 is 3.9, an R of 3.69 corresponds to a density of $\sim 2 \times 10^9$ cm^{-3}.

Absolute line-flux measurements provide a means for estimating a lower limit on active-region densities. Measured r-line fluxes (corrected for resonance scattering effects as in §IIIB1) convert to values of emission measure (the volume integral of n_e^2) in the field of view, that is, into emission measure per (arc minute)^2. Assuming that the line-of-sight dimension of the active region is also approximately one arc minute (an estimate that will not be grossly in error), the active-region volume in the field of view is 8.5×10^{28} cm^3. The derived emission measures ranged over 0.2-1.6×10^{48} cm^{-3}; the corresponding density range is 1.5-4.5×10^9 cm^{-3}. These approximate lower limits are in good agreement with the density inferred from the mean value of the R ratio.

R values for eight of the spectra were more than 2σ below the mean value of 3.69. This is a much smaller proportion of high-density regions than was found by McKenzie and Landecker (1982b) in a similar study with a smaller data set. They found measurable densities in 10 of 30 spectra. In Table 2, the high-density-region results are summarized for two assumed temperatures that bracket the active-region range. With the exception of 1878, the regions in which high-electron densities were measured were all productive of energetic solar flares. Although nonflare active-region densities are typically $< 3 \times 10^9$ cm^{-3}, higher values are occasionally observed, mostly in flare-productive regions.

11

Table 2. Active-Region Electron-Density Determinations

Date 1979	UT	Active Region	R	$n_e(1.2 \times 10^6$ K) 10^9 cm^{-3}	$n_e(1.8 \times 10^6$ K) 10^9 cm^{-3}
Mar 23	15:07	1638	3.29 ± 0.11	4.2 ± 0.1	5.2 ± 0.2
Mar 24	03:47	1638	3.43 ± 0.07	2.0 ± 0.1	3.7 ± 0.2
Mar 31	10:52	1661	3.28 ± 0.13	4.3 ± 0.2	5.3 ± 0.2
Apr 6	22:36	1661	3.30 ± 0.14	4.1 ± 0.2	5.0 ± 0.2
Apr 28	14:54	1705	3.27 ± 0.13	4.4 ± 0.2	5.4 ± 0.2
Jul 22	19:46	1878	3.40 ± 0.11	3.2 ± 0.1	4.0 ± 0.1
Aug 29	01:34	1943	3.33 ± 0.12	3.8 ± 0.2	4.7 ± 0.2
Sep 21	07:53	1994	3.06 ± 0.11	6.7 ± 0.2	7.9 ± 0.3

B.   TEMPERATURE DIAGNOSTICS

1.   O VII DIAGNOSTICS

The primary temperature diagnostic for use at temperatures around 2×10^6 K and lower is the R_1 ratio for O VII, calculated by Keenan, Kingston, and McKenzie (1985). This is the ratio of intensities of two resonance lines, the $1s^2$ ^{1}S - $1s3p$ ^{1}P line in the numerator and the r line in the denominator. McKenzie and Landecker (1982b) have shown that the r-line flux from active regions is depleted by resonance scattering in the outer corona. The resonance-scattering cross section is proportional to $f\lambda$, where f is the absorption oscillator strength and λ is the wavelength of the line in Å (Acton 1978). The $1s^2$ ^{1}S - $1s3p$ ^{1}P line flux (denoted r_1) will also be depleted by resonance scattering, in proportion to the product $f\lambda$. The G ratio for O VII provides a measure of the effects of resonance scattering. Only the r line, in the denominator of G, is affected; the f and i lines are both forbidden. Therefore, if G_0 is the value G would take in the absence of absorption, we

can correct the r line flux as follows:

$$r_{corr}/r = G/G_0 \qquad (4)$$

Similarly, it is easy to show that

$$(R_1)_{corr} = R_1(G_0/G)^{1-\alpha} \qquad (5)$$

where

$$\alpha = (f\lambda)_{r_1} / (f\lambda_r) \qquad (6)$$

McKenzie and Landecker (1982b) showed, and we show below, that $G_0 \approx 1.00$, and calculation shows that $\alpha = 0.18$ (Keenan, Kingston, and McKenzie, 1985). Accordingly, the R_1 ratios discussed below are all corrected with equation (5) using these values for the parameters. Making this correction assumes, in effect, that G is independent of temperature, and therefore introduces an error. This error is small. For example, Keenan, Tayal, and Kingston (1984b) calculated that G varies by a factor of 1.34 in the relatively wide temperature range of $1.0 - 1.8 \times 10^6$ K. This would correspond to a maximum error of 27% in R_1, arising from the application of equation 5. Figure 3 shows that the variation in G is predominantly attributable to resonance scattering.

R_1 values were determined for 78 of the spectra in the data sample. The results are shown in the histogram in Figure 2. Superimposed are the theoretical results of Keenan, Kingston, and McKenzie (1985). Of the 78 spectra, only one had an R_1 as high as 0.120, the calculated value for temperature T_m. The average value, 0.074, corresponds to a temperature of 1×10^6 K. This temperature determination is not credible because the emissivity of the O VII lines at 1×10^6 K is very low. We have estimated that uncertainties in the spectrometer response as a function of wavelength could lead to errors in the R_1 ratio as large as 20% (Keenan, Kingston, and McKenzie 1985). The errors in the calculations are hard to estimate because only a single group has done them, but it seems unlikely that these errors would be large enough
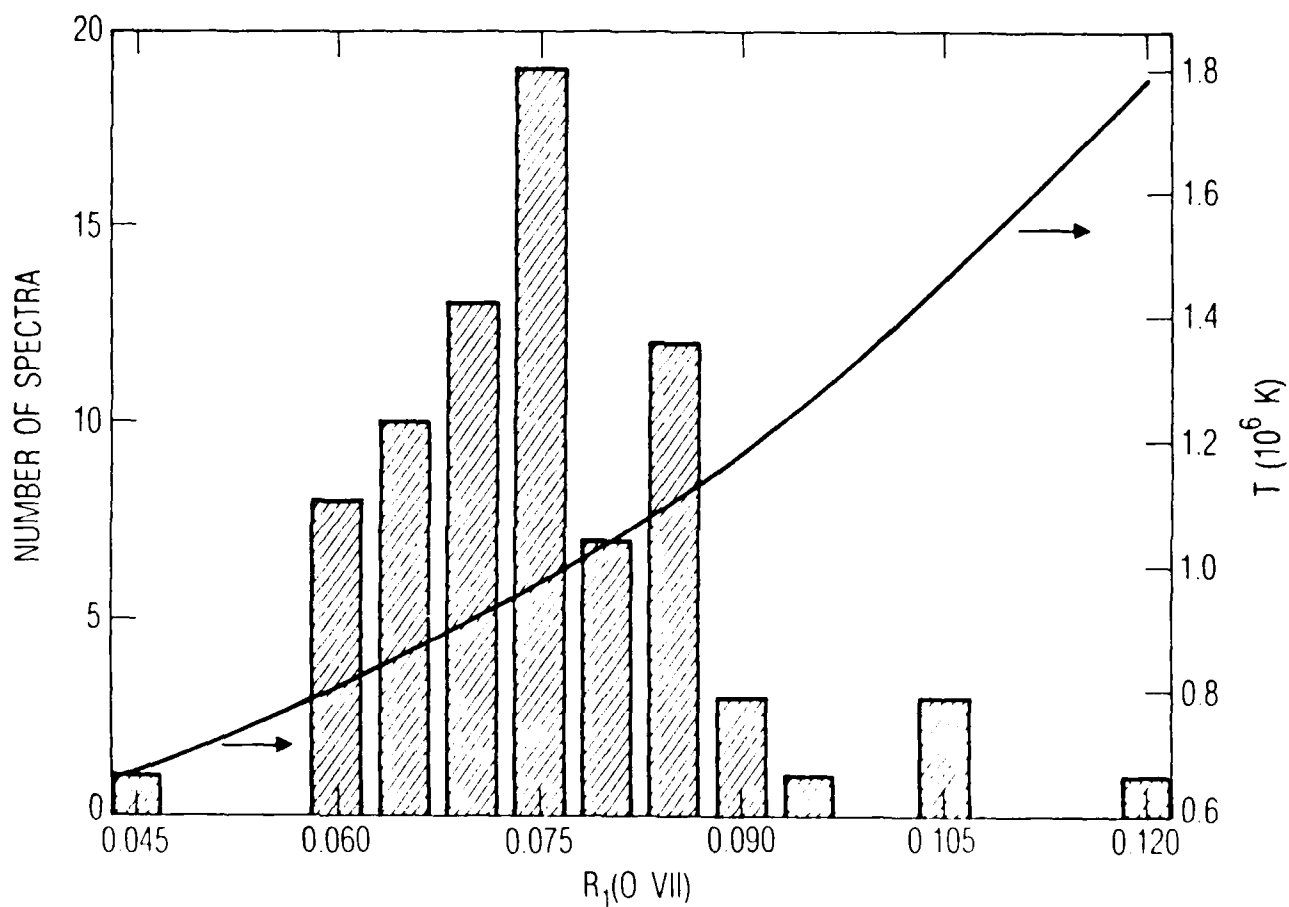
Figure 2: Histogram Showing the Occurrence of Measured Values of the R_1 Ratio for O VII. The numbers along the abscissa in this and other histograms in this report denote the bin centers. Calculated values of temperature are shown in the superimposed curve, which is from Keenan, Kingston, and McKenzie (1985).
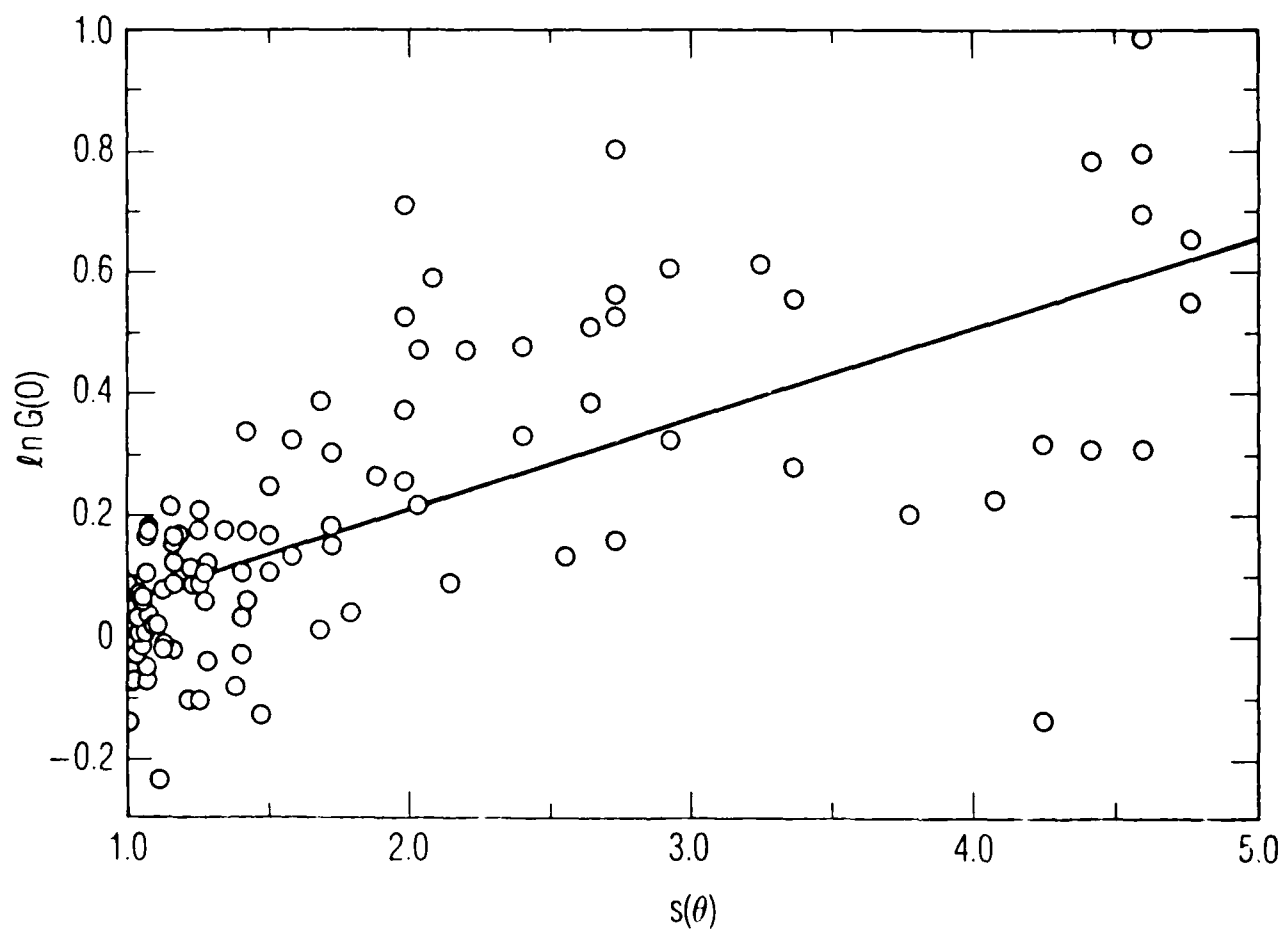
Figure 3: A plot of ln[G(O VII)] vs. s(θ), a Parameter That is Proportional
to the Optical Depth Through the Upper Corona to the O VII
Radiation Source for a Uniform Corona. Theta is the angle between
the line of sight and the inward normal to the solar surface.
Vertical error bars are typically ± 0.03. The line is a linear
least-squares fit to the relationship in equation (8).

15

($> 35\%$) to make the data consistent with temperatures higher than T_m. A measured temperature less than T_m indicates that the differential-emission measure function, $B(T)$, is decreasing with increasing temperature at T_m. Therefore, for most nonflaring active regions, the peak in the differential-emission measure function occurs at $T < 1.8 \times 10^6$ K.

The G ratio for O VII has been calculated a number of times, most recently by Pradhan (1982) and Keenan, Tayal, and Kingston (1984b). There is some disagreement between these two calculations for $T < 3 \times 10^6$ K, Pradhan's values being 10-20% higher. Keenan, Tayal, and Kingston (1984b) compared their calculations with Tokamak measurements by TFR Group, Doyle, and Schwob (1982); the agreement was remarkable. However, the Tokamak data were taken at plasma de sities of 10^{14} cm^{-3}. At such high densities the R ratio is zero and the G ratio becomes simply i/r. In addition, the two-photon $1s^2$ ^1S - $1s2s$ ^1S transition is quenched by collisional excitation from its upper state to the upper state of the r line. As a result, at $T = T_m$ the G ratio is about 13% lower than for coronal densities. When the TFR Group, Doyle, and Schwob (1982) results are corrected for this effect, with atomic data from Pradhan, Norcross, and Hummer (1981) and Lin, Johnson, and Dalgarno (1977), the results lie midway between the calculations of Pradhan (1982) and those of Keenan, Tayal, and Kingston (1984b) and cannot be used to discriminate between the two calculations.

G ratios for O VII were measured for 86 spectra. For most of them, G and R were determined simultaneously by the line-profile fitting process discussed in §IIIA. In a few cases a summing technique was used to determine the line strengths. The technique, described in McKenzie and Landecker (1982b), has been shown to give G ratios in agreement with those obtained by profile fitting. The results are displayed in Figure 3, in which $\ln[G(O\ VII)]$ is plotted against $s(\theta)$, where θ is the angle between the inward normal to the sun's surface at the active region being observed and the line of sight. The parameter $s(\theta)$, defined by McKenzie and Landecker (1982b), is proportional to the optical depth for resonance scattering for a uniform corona, so

$$G/G_0 \approx e^\tau \approx \exp[s(\theta) \int \kappa(z)dz] \qquad (7)$$

and

$$\ln(G) \approx [\int_{z}^{\infty} \kappa(z)dz]s(\theta) + \ln G_0 \qquad (8)$$

In these equations $\kappa(z)$ is the resonance-scattering absorption coefficient at height z in the corona. For small θ, $s(\theta) \approx \sec\theta$.

The line in Figure 3 is the least-squares fit to equation (8). Most of the variation in G can be attributed to resonance scattering. There is a great deal of scatter in the data, mostly because the corona is not a uniform shell at any given time and, over a time period as long as several months, can only be averaged as such. Because of resonance scattering, the G ratio for O VII is not useful for determining the temperature for individual spectra, but the fitted curve can be used to determine G_0 and hence an average temperature. The y-intercept gives $G_0 = 0.92$. However, for $\theta \approx 0$, scattering of r-line flux into the line of sight can be comparable to scattering out, so G might be increased or decreased depending on the geometry. Therefore, the $\theta = 0$ intercept may give a better estimate of G_0 than the $s = 0$ intercept. In this case, $G_0 = 1.07$. The G_0 range of 1.07 - 0.92 corresponds to a temperature range of $1.7-2.4 \times 10^6$ K according to Pradhan (1982) and $1.2-1.6 \times 10^6$ K according to Keenan, Kingston, and Tayal (1984b).

2. Ne IX DIAGNOSTICS

The G ratio is the most useful diagnostic in the temperature range $2-5 \times 10^6$ K, where emission from Ne IX is strong. This ratio has been calculated by Pradhan and Shull (1981), Pradhan (1982), Wolfson et al. (1983), Keenan, Tayal, and Kingston (1984c), and Keenan et al. (1987). The Wolfson et al. (1983) and Pradhan and Shull (1981) calculations yield temperatures above 10^7 K when applied to the data in this study and can therefore be discounted. The Keenan, Tayal, and Kingston (1984c) calculations have been superseded by the Keenan et al. (1987) results, so we need only consider these latter calculations and those of Pradhan (1982). Similar to the case of

17

O VII, the Pradhan calculations are 10-15% higher than those of Keenan et al.

The G ratio for Ne IX was measurable for 70 active-region spectra. The data are displayed in the histogram in Figure 4. The theoretical results of Keenan et al. (1987) and Pradhan (1982) are superimposed on the figure. Figure 5, a plot of G(Ne IX) vs G(O VII) for those spectra for which both could be measured, provides evidence that the highest G(Ne IX) values measured are significantly increased by resonance scattering of the r line radiation. Therefore, in Figure 4, the histogram shows data for which G(O VII) > 1.50 without cross-hatching. The G(Ne IX) for these spectra are likely to be significantly increased by resonance-scattering effects. For small values of G(O VII), G(Ne IX) values are concentrated in the range 0.80-0.95. This corresponds to the temperature range $2.2-3.8 \times 10^6$ K according to Keenan et al. (1987) and $3.6-5.5 \times 10^6$ K according to Pradhan (1982). For Ne IX, $T_m = 4.2 \times 10^6$ K.

The interpretation of these results depends on which theoretical calculation is deemed correct. The R_1 ratio for Ne IX provides us with a means for checking the general range of temperatures obtained from the G ratio. The $1s^2$ ^1S - $1s3p$ ^1P line is weak and blended and, consequently, can only be used with very intense spectra or spectra compiled by summing a number of weak ones. Keenan et al. (1987) analyzed a spectrum compiled by summing 271 individual SOLEX B spectral scans on nonflaring active regions. They found $\langle R_1 \rangle = 0.088 \pm 0.004$, which corresponds to a temperature of $\sim 1.9 \times 10^6$ K. For $T = T_m$, R_1 is equal to 0.132, 50% higher than the measured value. An error this large seems very unlikely in view of the good agreement between the Keenan et al. (1987) calculations and the data for the R_0 and G ratios.

These results favor the Keenan et al. G-ratio calculations, and imply that active-region temperatures derived from Ne IX ratios are lower than T_m and therefore that B(T) is a decreasing function of temperature in this range.

3. Mg XI DIAGNOSTICS

The G ratio is the most useful diagnostic for the temperature range in which Mg XI lines are strongest. The 3p line used in the R_1 ratio is very weak and lies near the end of the scanning range for the SOLEX B spectro-
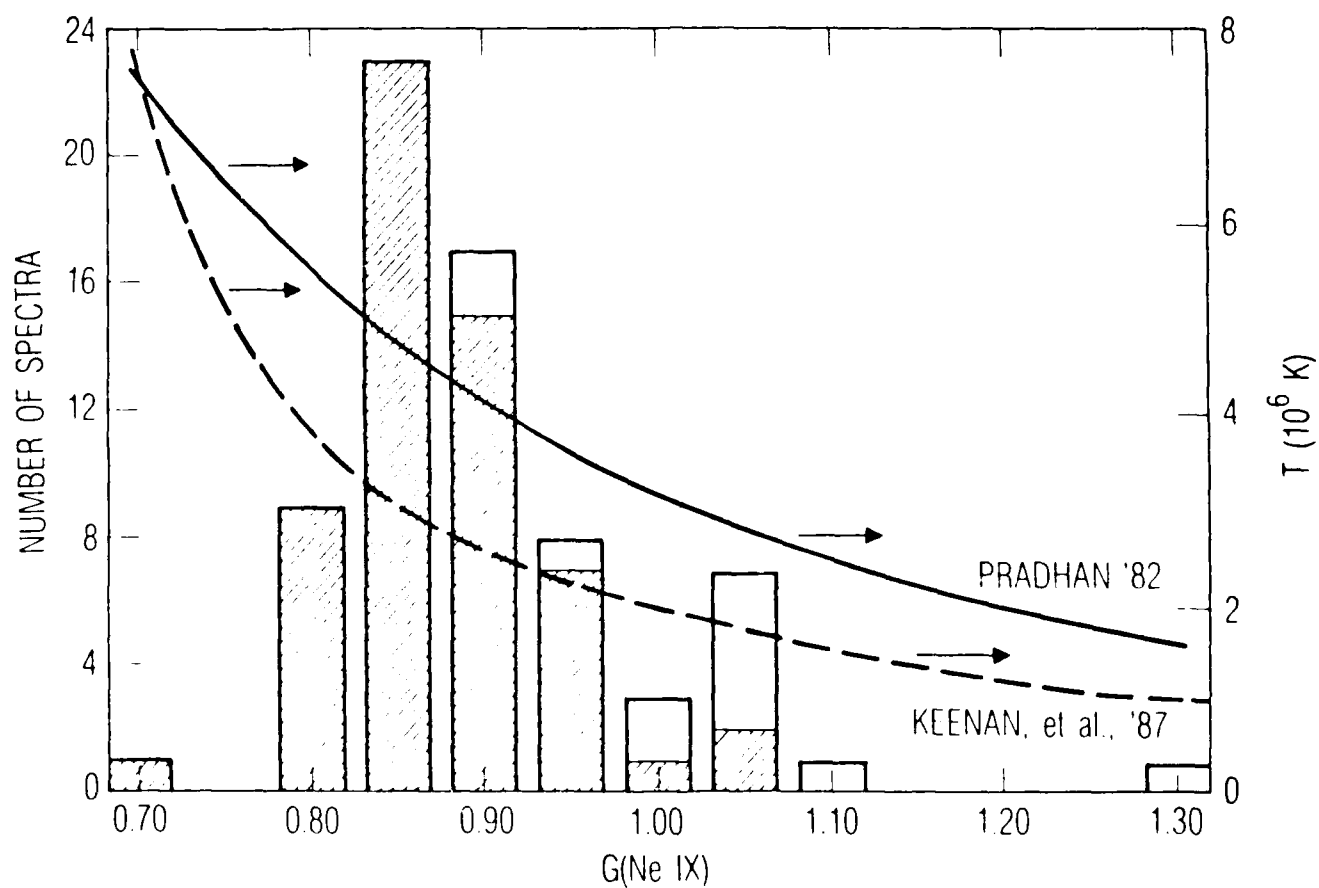
Figure 4. Histogram Showing the Occurrence of Measured Values of G(Ne IX).
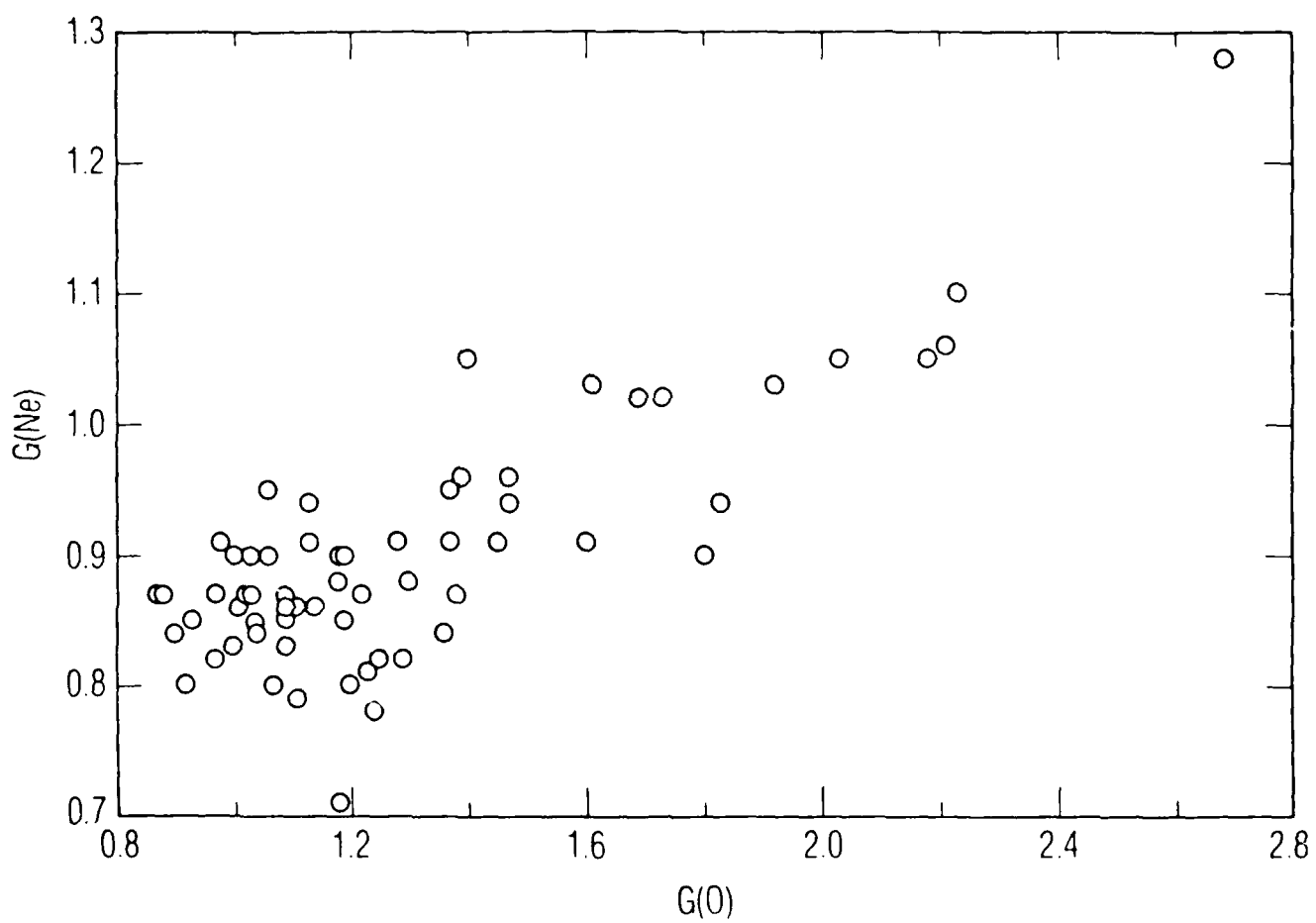Theoretical curves from Pradhan (1982) and Keenan et al. (1987) are
superimposed.

Figure 5. A Plot of G(Ne IX) vs. G(O VII). The correlation between the two
G ratios shows that resonance-scattering effects cannot be ignored
for Ne IX.

meter. Therefore, the R_1 ratio was not useful for the spectra treated here. Theoretical calculations of the G ratio have been made by Keenan, Tayal, and Kingston (1984a) and Wolfson et al. (1983). G values from the latter calculation are substantially higher than those from the former (e.g., 1.04 vs. 0.73 at 5×10^6 K). We choose the Keenan, Tayal, and Kingston (1984a) results for a number of reasons. First, the Wolfson et al. (1983) results yield implausibly high temperatures for a few of our active-region spectra. For example, the absence of detectable Fe XX emission shows that the Mg XI temperature cannot be over 10^7 K (Jordan 1970), as the Wolfson et al. results would indicate in these cases. Second, flare observations of G by McKenzie et al. (1985) and Wolfson et al. (1983) yield implausibly high temperatures when the Wolfson et al. calculations are applied. These flare observations might be explained under the assumption that the plasma was in an ionizing state, since ionizing plasmas have lower G values than plasmas in ionization equilibrium (Acton and Brown 1978). In some cases, the plasma would have to be ionizing even during the declining stages of the flares, and this is unlikely. Finally, the Keenan et al. (1987) R-matrix method has yielded plausible results for O VII and Ne IX, while the Wolfson et al. (1983) calculations for Ne IX could not be reconciled with the data.

The G ratio for Mg XI was measurable for only 43 spectra in our data sample. The reason for this is that the Mg XI emission was in most cases very weak. This weakness is reflected in relatively large uncertainties in the G ratio, when it could be determined at all. For O VII and Ne IX, typical statistical errors in G were ±3%, while those for Mg XI were ±10%. The data are plotted in Figure 6 with a format similar to that of Figure 4. Again the data for which G(O VII) > 1.50 are separately shown without cross-hatching, even though G(Mg XI) is not correlated with G(O VII) and no correlation is expected on theoretical grounds. The G ratios range from 0.70 to 1.30, with only two values higher than 1.00. The 1.00 - 0.70 G-ratio range corresponds to a temperature range of $3-6 \times 10^6$ K (Keenan, Tayal, and Kingston 1984a). For Mg XI, $T_m = 7 \times 10^6$ K (Mewe and Gronenschild 1981), so the Mg XI temperature is always lower than T_m. This means that B(T) is a declining function of temperature in this range. The two high values of G are 1.08 ± 0.14 and 1.30
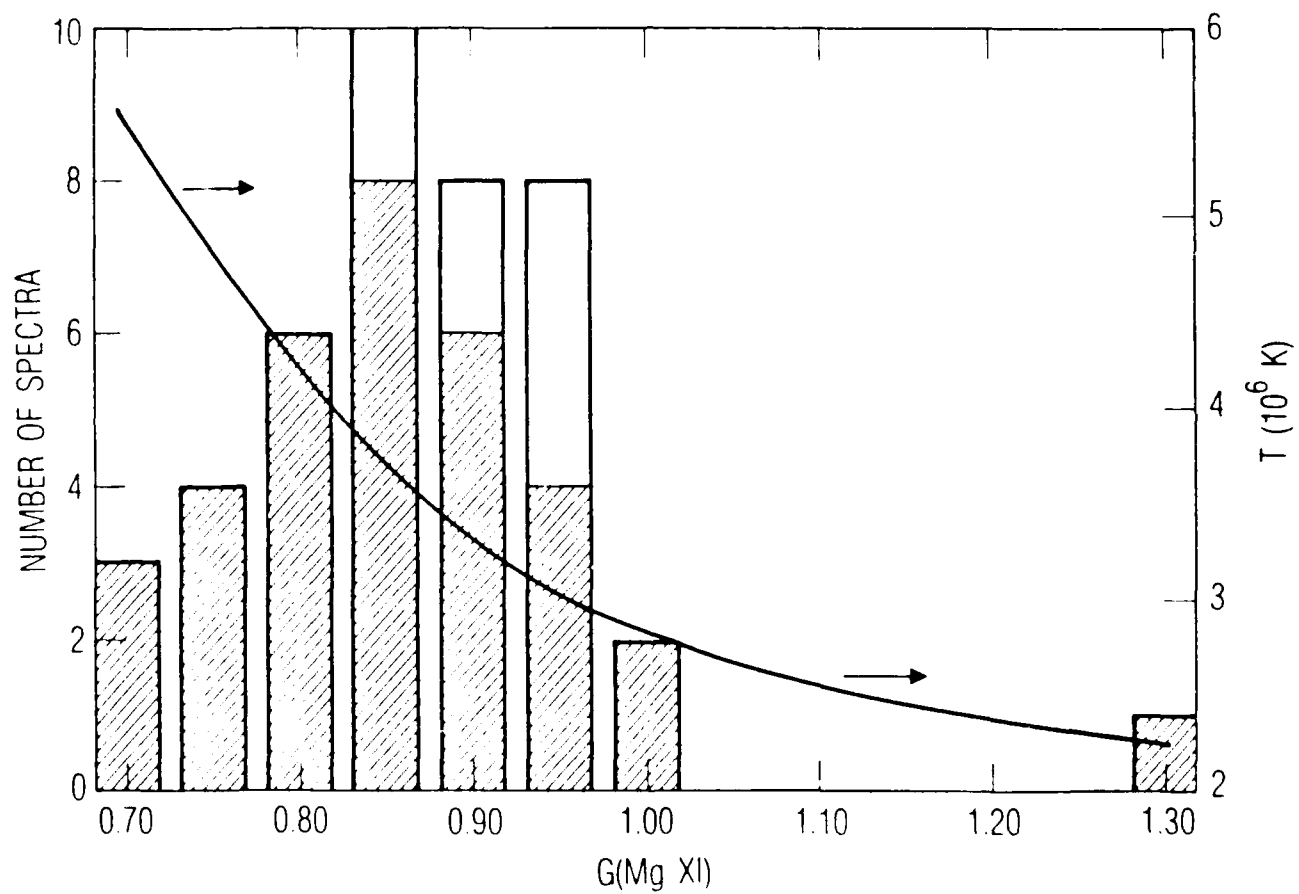
Figure 6. Histogram Showing the Occurrence of Measured Values of G(Mg XI).
Typical vertical error bars are ± 10%. The theoretical curve is
from Keenan, Tayal, and Kingston (1984a).

± 0.22. The latter corresponds to $T < 3.5 \times 10^6$ K (2σ upper limit). Temperatures below ~ 3×10^6 K are implausible because the Mg XI emissivities are very low.

4. SUMMARY OF THE TEMPERATURE MEASUREMENTS

The combination of the temperature measurements allows us to obtain a qualitative picture of the differential-emission-measure function, $B(T)$. $B(T)$ reaches a peak at $T < T_m(O\ VII) = 1.8 \times 10^6$ K, and at higher temperatures falls off with increasing T. In relatively rare cases the peak of $B(T)$ may occur at a temperature slightly higher than 1.8×10^6 K. The fall-off at higher temperatures is not necessarily monotonic, but there apparently is no temperature range wider than 2×10^6 K in which $B(T)$ is not generally declining with increasing temperature. The SOLEX spectrometers cannot locate the peak in $B(T)$, but grating spectrometers with which the C V lines can be measured, such as the Lockheed rocket instrument (Acton et al. 1985), may be able to do so.

C. SUMMARY OF THE COMPARISON OF THE LINE-RATIO CALCULATIONS WITH THE DATA

In the course of the analysis, the various theoretical calculations of the helium-like ion line ratios were evaluated. The G-ratio calculations of Pradhan (1982) and Keenan and his collaborators (Keenan, Tayal, and Kingston 1984a,b; Keenan et al. 1987) were acceptable, with the latter slightly preferred in the case of Ne IX. Pradhan (1982) did no calculations for Mg XI. The earlier calculations of Pradhan and Shull (1981) and Wolfson et al. (1983) were contradicted by the data. The agreement of the most recent calculations with the data not only allows us to use the calculated G ratios with confidence, but also indicates that the complexity of the latest and most sophisticated calculations is justified by the accuracy of the results.

For O VII, the R_0-ratio calculations by the authors cited above, and by Doyle, Tayal, and Kingston (1983) are all in good agreement with one another and are consistent with the solar active-region data. The data do not give us the means to determine the value of the parameter n_c, but all of the calculations agree on a value of ~ 3×10^{10} cm^{-3}. [Wolfson et al. (1983) did not

calculate n_c].

The R_1 ratios were calculated only by Keenan and his collaborators (Keenan, Kingston, and McKenzie 1985, 1986; Keenan et al. 1987). For O VII and Ne IX, R_1 gave lower temperatures than did G; the O VII temperatures were implausibly low in many cases. Part of this problem may be attributed to systematic errors in the measurements. Further observations and perhaps independent theoretical calculations will be needed to establish this potentially very useful diagnostic. The R_1 ratio for Mg XI could not be used in this study.

IV. DISCUSSION

The outstanding feature of solar active regions is bipolar magnetic field structure. Indeed, in his descriptive chapter in the Skylab Solar Workshop monograph Solar Active Regions, Sheeley (1981) describes an active region as "the totality of all phenomena accompanying the birth and early development of a solar magnetic region." He devotes the remaind r of the chapter to a description of "bipolar magnetic regions." Skylab x-ray photographs clearly show the confinement of hot plasmas to magnetic-field loop structures in the corona (e.g., Webb 1981). In addition to the distinguishable loops, there is usually faint and indistinct emission that cannot be unambiguously identified with measured photospheric fields. Nevertheless, it is likely that the great majority of the x-ray flux detected by the SOLEX spectrometers comes from plasmas confined in magnetic loops. The x-ray flux that arises outside of bipolar regions is undetectable by the spectrometers. In the following discussion, we assume that the active-region x-ray emission comes predominantly from plasmas confined in magnetic loops.

In viewing a region as large as a one-arc-minute square, the SOLEX B spectrometer observes the superimposed spectra from a large number of loops. This can be demonstrated as follows. Suppose the loops are large, with a typical length of 1 arc minute (4.4×10^9 cm) and a length-to-diameter ratio of 10. With a density of 3×10^9 cm^{-3}, the emission measure of a single such loop is 6×10^{45} cm^{-3}. The observed O VII resonance-line counting rates convert into emission measures on the order of 7×10^{47} cm^{-3}, depending upon the temperature and the assumed value of the coronal oxygen abundance [we use 7×10^{-4} for the O/H abundance ratio (Ross and Aller 1976)]. This means that ~ 100 loops would be in the SOLEX field of view at one time. If the loops are smaller, there would be more.

Jordan (1976) used simple loop models based upon observations to study loop energetics. Rosner, Tucker, and Vaiana (1978) modeled symmetric loops for which the conductive energy flux at the base was zero. The temperature increases from T_0 at the base of the loop to a maximum, T_1, at the apex. They

were able to derive an expression relating the loop half-length L, the pressure p, and T_1:

$$T_1 \approx 1.4 \times 10^3 (pL)^{1/3} \quad \text{(cgs units)} \tag{9}$$

Hood and Priest (1979) provide a good review of the theoretical work up until that time and then go on to present more sophisticated models. The conductive flux is a derived parameter instead of being fixed at zero, and T_1 becomes a function of three parameters: the loop length, the pressure at the base, and the mechanical heating. While the scaling equations are different from those of Rosner, Tucker, and Vaiana (1978), equation (9) can still serve in a discussion of our observations. According to the equation, a loop for which $T_1 = 1.5 \times 10^6$ K and the plasma density $n_e = 2 \times 10^9$ cm^{-3} would have $L = 1.5 \times 10^4$ km. The full length of such a loop would be 40 arc sec. The Hood and Priest (1979) results for stable loops are of similar magnitude.

One feature of the loops is particularly important. Most of the coronal plasma in a given loop is nearly isothermal at temperature T_1. This is true both of the observations (Jordan 1976) and the theoretical calculations of the differential emission measure (Rosner, Tucker, and Vaiana 1978). This means that B(T) can be approximated by

$$B(T)\Delta T = N(T)b(T)\Delta T \tag{10}$$

where $N(T)\Delta T$ is the number of loops in the field of view such that $T < T_1 < T + \Delta T$, and b(T) is the emission measure of a loop for which $T_1 = T$. The emission measure b(T) certainly increases with increasing T, if only because higher-temperature loops are longer and therefore have more volume. This means that for $T > T_m$(O VII), N(T) falls off very rapidly with increasing T. Thus the active-region structure is dominated by relatively low-temperature loops.

V. SUMMARY

Spectra from the SOLEX B RAP spectrometer have been used to analyze the temperature and density structure of over 100 nonflaring solar active regions. Density measurements that used the R ratio of O VII indicated that few regions have electron densities higher than $\sim 3 \times 10^9$ cm^{-3}. In a few cases, flare-productive regions had measured densities approximately twice this high. Temperature-sensitive line ratios in the helium-like ions O VII, Ne IX, and Mg XI enabled us to deduce the general properties of the differential emission measure function B(T) for nonflaring regions. B(T) falls off with increasing temperature above a peak temperature that is almost always lower than T_m(O VII) $= 1.8 \times 10^6$ K. This means that active regions are characterized by a large number of low-temperature coronal loops.

In the course of the study, we were also able to evaluate existing theoretical calculations of the helium-like ion line ratios. A number of them can now be rejected as inconsistent with the data. Future work may modify the conclusions of the study, but not significantly. For example, future calculations may indicate that the peak of B(T) occurs at slightly higher temperatures, but it is unlikely that the peak temperature is much higher than 2×10^6 K. Future observations, particularly of lines from helium-like C V, may allow experimenters to fix the peak temperature for B(T) more precisely.

REFERENCES

Acton, L. W. 1978, Ap. J., 225, 1069.

Acton, L. W., and Brown, W. A. 1978, Ap. J., 225, 1065.

Acton, L. W., Bruner, M. E., Brown, W. A., Fawcett, B. C.,
    Schweizer, W., and Speer, R. J. 1985, Ap. J., 291, 865.

Acton, L. W., Catura, R. C., Meyerott, A. J., Wolfson, C. J.,
    and Culhane, J. L. 1972, Solar Phys., 26, 183.

Batstone, R. M., Evans, K., Parkinson, J., and Pounds, K. A.
    1970, Solar Phys., 13, 389.

Doschek, G. A. 1972, Space Sci. Revs., 13, 765.

Doyle, J. G., Tayal, S. S., and Kingston, A. E. 1983,
    M. N. R. A. S., 203, 31P.

Finn, G. D., and Mugglestone, D. 1965, M. N. R. A. S., 129, 221.

Gabriel, A. H., and Jordan, C. 1969, M. N. R. A. S., 145, 241.

Hood, A. W., and Priest, E. R. 1979, Astr. Ap., 77, 233.

Hutcheon, R. J., Pye, J. P., and Evans, K. D. 1976a, Astr. Ap.,
    51, 451.

_____. 1976b, M. N. R. A. S., 175, 489.

Jordan, C. 1970, M. N. R. A. S., 148, 17.

_____. 1976, Phil. Trans. R. Soc. London A, 281, 391.

Keenan, F. P., Kingston, A. E., and McKenzie, D. L. 1985, Ap.
    J., 291, 855.

_____. 1986, Ap. J., 303, 486.

Keenan, F. P., McKenzie, D. L., McCann, S. M., and Kingston, A. E. 1987,
    Ap. J., in press.

Keenan, F. P., Tayal, S. S., and Kingston, A. E. 1984a,
    M. N. R. A. S., 207, 51P.

_____. 1984b, Solar Phys., 92, 75.

_____. 1984c, Solar Phys., 94, 85.

Landecker, P. B., McKenzie, D. L., and Rugge, H. R. 1979, SPIE
    Proc., 184, 285.

Lin, C. D., Johnson, W. D., and Dalgarno, A. 1977, Phys. Rev. A,
    15, 154.

McKenzie, D. L., Broussard, R. M., Landecker, P. B., Rugge, H. R., Young,
    R. M., Doschek, G. A., and Feldman, U. 1980, Ap. J. (Letters), 238, L43.

McKenzie, D. L., and Landecker, P. B. 1982a, Ap. J., 254, 309.

_____. 1982b, Ap. J., 259, 372.

McKenzie, D. L., Landecker, P. B., Broussard, R. M., Rugge, H.
    R., Young, R. M., Feldman, U., and Doschek, G. A. 1980, Ap. J., 241, 407.

McKenzie, D. L., Landecker, P. B., Feldman, U., and Doschek, G.
    A. 1985, Ap. J., 289, 849.

Mewe, R., and Gronenschild, E. H. B. M. 1981, Astr. Ap. Suppl., 45, 11.

Neupert, W. M., Gates, W., Swartz, M., and Young, R. M. 1967,
    Ap. J. (Letters), 149, L79.

Parkinson, J. H. 1975, Solar Phys., 42, 183.

Pradhan, A. K. 1982, Ap. J., 263, 477.

Pradhan, A. K., Norcross, D. W., and Hummer, D. G. 1981, Ap. J., 246, 1031.

Pradhan, A. K., and Shull, J. M. 1981, Ap. J., 249, 821.

Rosner, R., Tucker, W. H., and Vaiana, G. S. 1978, Ap. J., 220, 643.

Ross, J. E., and Aller, L. H. 1976, Science, 191, 1223.

Sheeley, N. R., Jr. 1981, Solar Active Regions, ed. F. Q. Orrall
    (Boulder: Colorado Assoc. Univ. Press), p 17ff.

Siarkowski, M., Sylwester, J., Bromboszcz, G., Korneev, V. V.,
    Mandelshtam, S. L., Oparin, S. N., Urnov, A. M., Zhitnik, I. A., and
    Vasha, S. 1982, Solar Phys., 77, 183.

TFR Group, Doyle, J. G., and Schwob, J. L. 1982, J. Phys. B, 15, 813.

Webb, D. F. 1981, Solar Active Regions, ed. F. Q. Orrall
    (Boulder: Colorado Assoc. Univ. Press), p 165ff.

Wolfson, C. J., Doyle, J. G., Leibacher, J. W., and Phillips, K.
    J. H. 1983, Ap. J., 269, 319.

LABORATORY OPERATIONS

The Aerospace Corporation functions as an "architect-engineer" for
national security projects, specializing in advanced military space systems.
Providing research support, the corporation's Laboratory Operations conducts
experimental and theoretical investigations that focus on the application of
scientific and technical advances to such systems. Vital to the success of
these investigations is the technical staff's wide-ranging expertise and its
ability to stay current with new developments. This expertise is enhanced by
a research program aimed at dealing with the many problems associated with
rapidly evolving space systems. Contributing their capabilities to the
research effort are these individual laboratories:

Aerophysics Laboratory: Launch vehicle and reentry fluid mechanics, heat
transfer and flight dynamics; chemical and electric propulsion, propellant
chemistry, chemical dynamics, environmental chemistry, trace detection;
spacecraft structural mechanics, contamination, thermal and structural
control; high temperature thermomechanics, gas kinetics and radiation; cw and
pulsed chemical and excimer laser development including chemical kinetics,
spectroscopy, optical resonators, beam control, atmospheric propagation, laser
effects and countermeasures.

Chemistry and Physics Laboratory: Atmospheric chemical reactions,
atmospheric optics, light scattering, state-specific chemical reactions and
radiative signatures of missile plumes, sensor out-of-field-of-view rejection,
applied laser spectroscopy, laser chemistry, laser optoelectronics, solar cell
physics, battery electrochemistry, space vacuum and radiation effects on
materials, lubrication and surface phenomena, thermionic emission, photo-
sensitive materials and detectors, atomic frequency standards, and
environmental chemistry.

Computer Science Laboratory: Program verification, program translation,
performance-sensitive system design, distributed architectures for spaceborne
computers, fault-tolerant computer systems, artificial intelligence, micro-
electronics applications, communication protocols, and computer security.

Electronics Research Laboratory: Microelectronics, solid-state device
physics, compound semiconductors, radiation hardening; electro-optics, quantum
electronics, solid-state lasers, optical propagation and communications;
microwave semiconductor devices, microwave/millimeter wave measurements,
diagnostics and radiometry, microwave/millimeter wave thermionic devices;
atomic time and frequency standards; antennas, rf systems, electromagnetic
propagation phenomena, space communication systems.

Materials Sciences Laboratory: Development of new materials: metals,
alloys, ceramics, polymers and their composites, and new forms of carbon; non-
destructive evaluation, component failure analysis and reliability; fracture
mechanics and stress corrosion; analysis and evaluation of materials at
cryogenic and elevated temperatures as well as in space and enemy-induced
environments.

Space Sciences Laboratory: Magnetospheric, auroral and cosmic ray
physics, wave-particle interactions, magnetospheric plasma waves; atmospheric
and ionospheric physics, density and composition of the upper atmosphere,
remote sensing using atmospheric radiation; solar physics, infrared astronomy,
infrared signature analysis; effects of solar activity, magnetic storms and
nuclear explosions on the earth's atmosphere, ionosphere and magnetosphere;
effects of electromagnetic and particulate radiations on space systems; space
instrumentation.

END

DATE

FILMED

DTIC

JULY 88